

individually off the trapped electrons which are still periodically deployed in space (that is, still k -matched to forward scattering) but having a range of momenta producing, therefore, a range of scattered frequencies¹⁷. Also, the Doppler shifts²⁸ expected for electrons moving at, say, a relativistic $\gamma \approx 4$ within a range of angles corresponding to $f/5$ focusing is approximately ω_p and nearly symmetric on the red and blue sides of the satellites which could further explain the ‘filling in’ of the satellites.

Figure 2 shows the measured electron energy spectra corresponding to the two optical spectra in Fig. 1 plus an intermediate plasma density of $1.0 \times 10^{19} \text{ cm}^{-3}$. The number of accelerated electrons at a given energy and the maximum electron energy both show a dramatic increase as the plasma density is increased to $1.5 \times 10^{19} \text{ cm}^{-3}$: the number of electrons above 20 MeV increases by at least two orders of magnitude and the accelerated electron distribution is rather flat up to 30 MeV where it begins to decrease with energy up to 44 MeV, which is the spectrometer limit. We interpret this sudden increase in accelerated electrons and maximum energy, together with the broadening of the electromagnetic spectrum, as the signature that wave-breaking has occurred. The large increase in the number of electrons accelerated at the highest plasma density is consistent with the wave trapping the bulk of the plasma thermal distribution function rather than a few tail particles at low plasma densities. Indeed the (spectrometer-limited) maximum electron energy of 44 MeV is not too far from the absolute maximum of 70 MeV that a test electron would obtain, limited by dephasing in an ideal plasma wave with $\alpha = 1$ which is near the relativistic warm-plasma wave-breaking limit expected for our plasma conditions.

We note that the normalized transverse emittance $\epsilon_n = \gamma \sigma \delta\theta$ of any particular energy group from this experiment is quite small. Here γ is the relativistic Lorentz factor for that energy group, σ is the source size ($\sim 10 \mu\text{m}$), and $\delta\theta$ the angular spread ($\sim 8 \text{ mrad}$ due to the $f/60$ collection). At 30 MeV, $\epsilon_n = 5\pi \text{ mm mrad}$ which is low enough to be competitive with modern photoinjector-based linacs²⁹. However, the beam current measured here ($\sim 1 \text{ A}$ in a $\pm 1\%$ bandwidth around 30 MeV) is roughly 10–100 times lower than present-day photoinjector technology. The tremendous advantage over conventional linacs is the extremely short distance over which this energy is obtained. As dephasing limits the acceleration length to $\pi \gamma^3 / k_0 \approx 300 \mu\text{m}$, the 44 MeV that the electrons gain indicate a peak electric field of over 100 GV m^{-1} which would represent the higher collective wave field ever produced in a laboratory. Given that laser technology, including repetition rate, average power, efficiency and smaller packaging is advancing very rapidly, it is reasonable to expect that the average current can be increased through a combination of higher laser frequencies and plasma densities as well as by increased repetition rate. Thus, one could envisage in the not-too-distant future a new class of compact accelerators based on the breaking of relativistic electron plasma waves which may find applications where 2–200 MeV electrons or photons are needed. □

Received 15 May; accepted 19 September 1995.

1. Stix, T. H. *The Theory of Plasma Waves* (McGraw-Hill, New York, 1962).
2. Dawson, J. M. *Scient. Am.* **260**, 54–61 (1989).
3. Tajima, T. & Dawson, J. M. *Phys. Rev. Lett.* **45**, 267–270 (1979).
4. Joshi, C. et al. *Nature* **311**, 525–529 (1984).
5. Dawson, J. M. *Phys. Rev.* **113**, 383–387 (1959).
6. Coffey, T. P. *Phys. Fluids* **14**, 1402–1406 (1971).
7. Akhiezer, A. I. & Polovin, R. V. *Sov. Phys. JETP* **3**, 696–699 (1956).
8. Katsouleas, T. & Mori, W. B. *Phys. Rev. Lett.* **61**, 90–93 (1988).
9. Forslund, D. W., Kindel, J. M. & Lindman, E. L. *Phys. Fluids* **18**, 1002–1016 (1975).
10. Mori, W. B., Decker, L. D., Hinkel, D. E. & Katsouleas, T. *Phys. Rev. Lett.* **72**, 1482–1485 (1994).
11. Chen, F. F. *Phys. Scripta* **T30**, 14–23 (1990).
12. Joshi, C., Tajima, T., Dawson, J. M., Baldis, H. A. & Ebrahim, N. A. *Phys. Rev. Lett.* **47**, 1285–1288 (1981).
13. Turner, R. E. et al. *Phys. Rev. Lett.* **57**, 1725–1728 (1986).
14. Batha, S. H. et al. *Phys. Rev. Lett.* **66**, 2324–2327 (1991).
15. Nakajima, K. et al. *Phys. Rev. Lett.* **74**, 4428–4431 (1995).
16. Coverdale, C. A. et al. *Phys. Rev. Lett.* **74**, 4659–4662 (1995).
17. Everett, M. J. et al. *Phys. Rev. Lett.* **74**, 1355–1358 (1995).
18. Sprangle, P., Esarey, E., Ting, A. & Joyce, G. *Appl. Phys. Lett.* **53**, 2146–2148 (1988).
19. Sessler, A. M. *Physics Today* **41**, 26–34 (1988).
20. Kitagawa, Y. et al. *Phys. Rev. Lett.* **68**, 48–51 (1992).
21. Clayton, C. E. et al. *Phys. Rev. Lett.* **70**, 37–40 (1993).
22. Everett, M. et al. *Nature* **368**, 527–529 (1994).
23. Ebrahim, N. A. *J. appl. Phys.* **76**, 7645–7647 (1994).
24. Decker, C. D., Mori, W. B. & Katsouleas, T. *Phys. Rev. E* **50**, R3338–R3341 (1994).
25. Tzeng, K.-C., Mori, W. B. & Decker, C. D. *Phys. Rev. Lett.* (submitted).
26. Danson, C. N. et al. *Opt. Commun.* **103**, 392–397 (1993).
27. Brückner, R. thesis, Univ. Orléans (1994).
28. Jackson, J. D. *Classical Electrodynamics* (Wiley, New York, 1975).
29. Fraser, J. S. & Sheffield, R. L. *IEEE J. quant. Electr.* **23**, 1489–1496 (1987).

20. Kitagawa, Y. et al. *Phys. Rev. Lett.* **68**, 48–51 (1992).
21. Clayton, C. E. et al. *Phys. Rev. Lett.* **70**, 37–40 (1993).
22. Everett, M. et al. *Nature* **368**, 527–529 (1994).
23. Ebrahim, N. A. *J. appl. Phys.* **76**, 7645–7647 (1994).
24. Decker, C. D., Mori, W. B. & Katsouleas, T. *Phys. Rev. E* **50**, R3338–R3341 (1994).
25. Tzeng, K.-C., Mori, W. B. & Decker, C. D. *Phys. Rev. Lett.* (submitted).
26. Danson, C. N. et al. *Opt. Commun.* **103**, 392–397 (1993).
27. Brückner, R. thesis, Univ. Orléans (1994).
28. Jackson, J. D. *Classical Electrodynamics* (Wiley, New York, 1975).
29. Fraser, J. S. & Sheffield, R. L. *IEEE J. quant. Electr.* **23**, 1489–1496 (1987).

ACKNOWLEDGEMENTS. We thank C. Stenz and R. Brückner for the design of the gas jet nozzle. Our particular thanks are due to W. B. Mori for many discussions and K-C. Tzeng for access to unpublished PIC simulation results. This work was supported by the EPSRC, the EU and the US Department of Energy.

Modelling urban growth patterns

Hernán A. Makse*, Shlomo Havlin**† & H. Eugene Stanley*

* Center for Polymer Studies and Department of Physics, Boston University, Boston, Massachusetts 02215, USA

† Department of Physics, Bar-Ilan University, Ramat-Gan, Israel

CITIES grow in a way that might be expected to resemble the growth of two-dimensional aggregates of particles, and this has led to recent attempts^{1–3} to model urban growth using ideas from the statistical physics of clusters. In particular, the model of diffusion-limited aggregation^{4,5} (DLA) has been invoked to rationalize the apparently fractal nature of urban morphologies¹. The DLA model predicts that there should exist only one large fractal cluster, which is almost perfectly screened from incoming ‘development units’ (representing, for example, people, capital or resources), so that almost all of the cluster growth takes place at the tips of the cluster’s branches. Here we show that an alternative model, in which development units are correlated rather than being added to the cluster at random, is better able to reproduce the observed morphology of cities and the area distribution of sub-clusters ('towns') in an urban system, and can also describe urban growth dynamics. Our physical model, which corresponds to the correlated percolation model^{6–8} in the presence of a density gradient⁹, is motivated by the fact that in urban areas development attracts further development. The model offers the possibility of predicting the global properties (such as scaling behaviour) of urban morphologies.

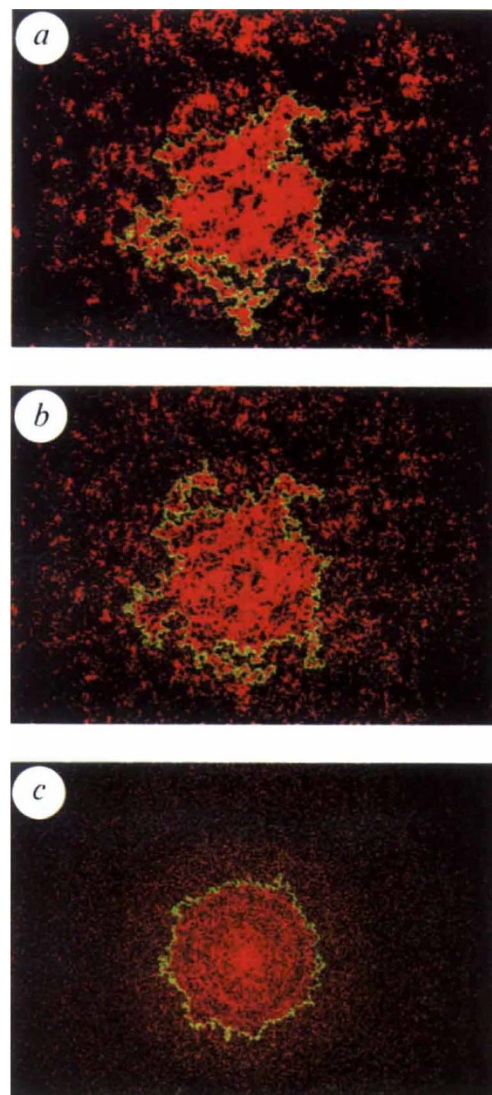
In the model we now develop we take into account two points. First, data on the population density $\rho(r)$ of actual urban systems are known to conform to the relation¹⁰ $\rho(r) = \rho_0 e^{-\lambda r}$, where r is the radial distance from the compact core, and λ is the density gradient. Therefore, in our model the development units are positioned with an occupancy probability $p(r) \equiv \rho(r)/\rho_0$ that behaves in the same fashion as is seen in observations of real cities. Second, in actual urban systems, the development units are not positioned at random. Rather, there exist correlations arising from the fact that when a development unit is located in a given place, the probability of adjacent development units increases; each site is not independently occupied by a development unit, but is occupied with a probability that depends on the occupancy of the neighbourhood.

In order to quantify these ideas, we use the correlated percolation model^{6–8}. In the limit where correlations are so small as to be negligible^{11,12}, a site at position \mathbf{r} is occupied if the occupancy variable $u(\mathbf{r})$ —an uncorrelated random number—is smaller than the occupation probability $p(\mathbf{r})$. To introduce correlations among the variables, we convolute the uncorrelated variables $u(\mathbf{r})$ with a suitable power-law kernel⁷, and define a new set of random variables $\eta(\mathbf{r})$ with long-range power-law correlations that decay as $r^{-\alpha}$, where $r \equiv |\mathbf{r}|$. The assumption of power-law interactions is motivated by the fact that the ‘decision’ for a

development unit to be placed in a given location decays gradually with the distance from an occupied neighbourhood. The correlation exponent α is the only parameter to be determined by empirical observations.

To discuss the morphology of a system of cities generated in the present model, we show in Fig. 1 our simulations of correlated urban systems for a fixed value of the density gradient λ , and for different degrees of correlation. The correlations have the effect of agglomerating the units around an urban area. In the simulated systems the largest occupation density is situated in the core (which acts as an 'attractive' centre of the city), and this is surrounded by small clusters or 'towns'. (In previous work^{1–3} the compact core has been called the central business district (CBD).) The correlated clusters are fairly compact near their respective centres and become less compact near their boundaries, in qualitative agreement with empirical data on real large cities such as Berlin, Paris and London^{1,13}.

The urban boundary of the largest city is defined to be the perimeter of the connected cluster connected to the CBD. As $p(r)$ decreases as one moves away from the core, the probability that the largest cluster remains connected decreases with r . The mean distance of the perimeter from the centre r_f is determined by the value of r for which $p(r)$ equals the percolation threshold—that is, $p(r_f) = p_c$, so $r_f = \lambda^{-1} \ln(1/p_c)$ (ref. 9).



The urban boundary in the model has the scaling properties of the external perimeter of a correlated percolation cluster in the presence of a gradient. The scaling of the length of the boundary within a region of size l , $L(l) \approx l^{D_e}$, defines the fractal dimension D_e , which we calculate to have values $D_e \approx 1.3$ for the uncorrelated case, and $D_e \approx 1.4$ for strong correlations ($\alpha \rightarrow 0$). Both values are consistent with actual urban data, for which values of D_e between 1.2 and 1.4 are measured¹. Near the frontier and on length scales smaller than the width of the frontier, the largest cluster has fractal dimension $d_f \approx 1.9$, as defined by the 'mass-radius' relation¹², independent of the correlations.

So far, we have argued how correlations between occupancy probabilities can account for the irregular morphology of towns in an urban system. As can be seen in Fig. 2a, the towns surrounding a large city like Berlin are characterized by a wide range of sizes. We are interested in the laws that quantify the town size distribution $N(A)$, where A is the area occupied by a given town, so we calculate the actual distribution of the areas of the urban settlements around Berlin and London. We find (Fig. 3a) that for both cities, $N(A)$ follows a power law.

This result can be understood in the context of our model. The small clusters surrounding the largest cluster are all situated at distances r from the CBD such that $p(r) < p_c$ or $r > r_f$. Therefore, we find $N(A)$, the cumulative area distribution of clusters

FIG. 1 a–c, Simulations of urban systems for different degrees of correlations. Red indicates the urban areas, and light green shows the external perimeter or urban boundary of the largest cluster connected to the CBD. In all the panels, we fix the value of the density gradient to be $\lambda = 0.009$. a, b, Two different examples of interactive systems of cities for correlation exponents $\alpha = 0.6$ and $\alpha = 1.4$, respectively. The development units are positioned with a probability that decays exponentially with the distance from the core. The units are located not randomly as in percolation, but rather in a correlated fashion depending on the neighbouring occupied areas. The correlations are parametrized by the exponent α . The strongly correlated case corresponds to small α ($\alpha \rightarrow 0$). When $\alpha > d$, where d is the spatial dimension of the substrate lattice ($d = 2$ in our case), we recover the uncorrelated case. Notice the tendency to more compact clusters as we increase the degree of correlations ($\alpha \rightarrow 0$). c, As a zeroth-order approximation, one might consider the morphology predicted in the extreme limit when development units are positioned at random, rather than in the correlated way shown in a and b. The results for this crude approximation of a non-interactive (uncorrelated) system of cities clearly display a drastically different morphology than found from data on real cities (such as shown in Fig. 2a). The non-interactive limit looks unrealistic in comparison with real cities, for the lack of interactions creates an urban area characterized by many small towns spread loosely around the core.

of area A , to be

$$N(A) \equiv \int_0^{p_c} n(A, p) dp \sim A^{-(\tau + 1/d_v)} \quad (1)$$

Here, $n(A, p) \sim A^{-\tau} g(A/A_0)$ is defined to be the average number of clusters containing A sites for a given p at a fixed distance r , and $\tau = 1 + 2/d_r$. Here, $A_0(r) \sim |p(r) - p_c|^{-d/d_v}$ corresponds to the maximum typical area occupied by a cluster situated at a distance r from the CBD, and $g(A/A_0)$ is a scaling function that decays rapidly (exponentially) for $A > A_0$. The exponent $v = v(\alpha)$ is defined by $\xi(r) \sim |p(r) - p_c|^{-v}$, where $\xi(r)$ is the connectedness length that represents the mean linear size of a cluster at a distance $r > r_f$ from the CBD.

In our numerical simulations we find a drastic increase of $v(\alpha)$ with the increase of the long-range correlations ($\alpha \rightarrow 0$) (Fig. 3b)⁸. The exponent $v(\alpha)$ affects the area distribution of the small clusters around the CBD (Fig. 3c), as specified by equation (1), and can be used to quantify the degree of interaction between the CBD and the small surrounding towns. For instance, for a strongly correlated system of cities characterized by small α , $v(\alpha)$ is large so that the area $A_0(r)$ and the linear size $\xi(r)$ of the towns will be large even for towns situated far from the CBD. This effect is observed in the correlated systems of cities of Fig. 1.

In Fig. 3a we also plot the power law for the area distribution predicted by equation (1) along with the real data for Berlin and London. We find that the slopes of the plots for both cities are consistent with the prediction (dashed line) for the case of highly

correlated systems, indicating qualitative agreement between the morphology of actual urban areas and the strongly correlated urban systems obtained in our simulations. Clearly, the exponent of the area distribution provides a stronger test of our model against observations than does the fractal dimension D_c of the perimeter.

We now discuss a generalization of our static model to describe the dynamics of urban growth. Empirical studies¹⁰ of the population density profile of cities show a remarkable pattern of decentralization, which is quantified by the decrease of $\lambda(t)$ with time (see Table 4 in ref. 14). The dynamics in the model (see Fig. 4) are quantified by a decreasing $\lambda(t)$, as occurs in actual urban areas. These considerations are tested in Fig. 2b, which shows our dynamical urban simulations of a strongly interacting system of cities characterized by a correlation exponent $\alpha = 0.05$ for three different values of λ . Qualitative agreement is observed between the morphology of the cities and towns of the actual data of Fig. 2a and the simulations of Fig. 2b.

We wish to comment on the coincidence between the settlement area distribution for different cities and different years (Berlin 1920 and 1945, and London 1981). We first note that these distributions are calculated on length scales larger than the domain of influence of any local planning constraint imposed on the growth of the cities. This fact, together with the fact that interactions among development units can be modelled by a scale-invariant power law, implies that the area distribution $N(A)$ is not affected by the effects of local growth restraints. A more detailed study (for example, calculating $N(A)$ only for those settlements under the domain of influence of applied local

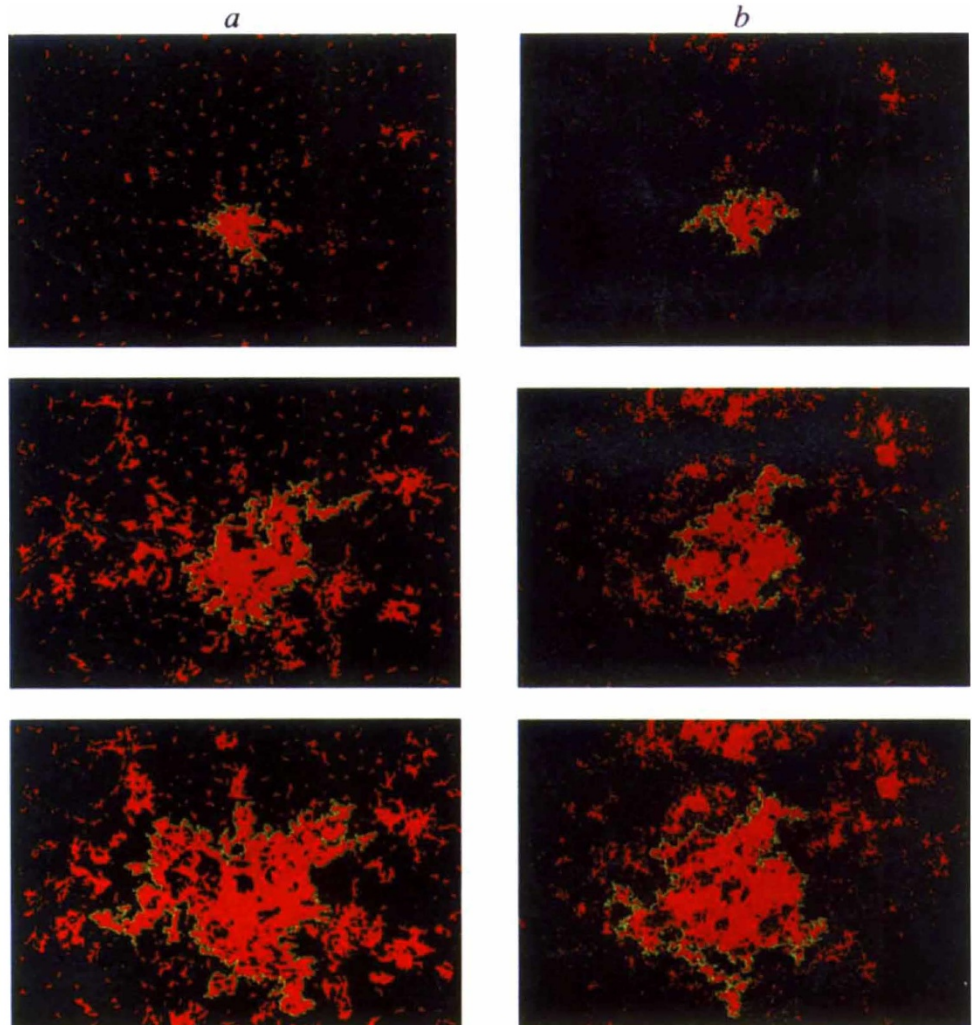


FIG. 2 Qualitative comparison between the actual urban data and the proposed model. *a*, Three steps of the growth with time of Berlin and surrounding towns. Data are shown for the years 1875, 1920 and 1945 (from top to bottom). *b*, Dynamical urban simulations of the proposed model. We fix the value of the correlation exponent to be $\alpha = 0.05$ (strongly correlated case), and choose the occupancy probability $p(r)$ to correspond to the density profiles shown in Fig. 4. We use the same seed for the random-number generator in all panels.

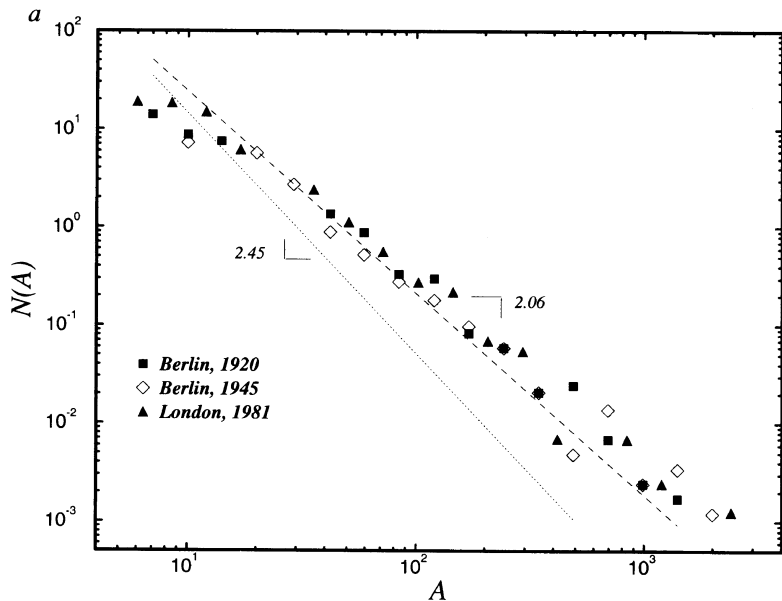


FIG. 3 a, Log-log plot of the area distribution $N(A)$ of the actual towns around Berlin and London. We first digitize the empirical data of Fig. 4.1 of ref. 13 (Berlin 1920 and 1945, shown in the last two panels of Fig. 2a), and Fig. 10.8 of ref. 1 (London 1981). Then, we count the number of towns that are covered by A sites, putting the result in logarithmically spaced bins (of size 1.2^k , with $k = 1, 2, \dots, 16$), and averaging over the size of the bin. A power law is observed for the area distributions of both urban systems. The dotted line shows the predictions of our model for the uncorrelated case (slope, 2.45), while the dashed line gives results for the strongly correlated case (slope, 2.06). Note that the area distributions for both cities agree much better with the strongly correlated case ($\alpha \rightarrow 0$). b, Connectedness length exponent $v(\alpha)$ as a function of the correlation exponent α . c, Log-log plot of the area distribution $N(A)$ calculated for the present model for different degrees of correlation. From top to bottom, $\alpha = 0.2$, $\alpha = 0.8$, $\alpha = 1.4$, and uncorrelated case. The linear fits correspond to the predictions of equation (1) using the values of $v(\alpha)$ from b, and $d_f = 1.9$.

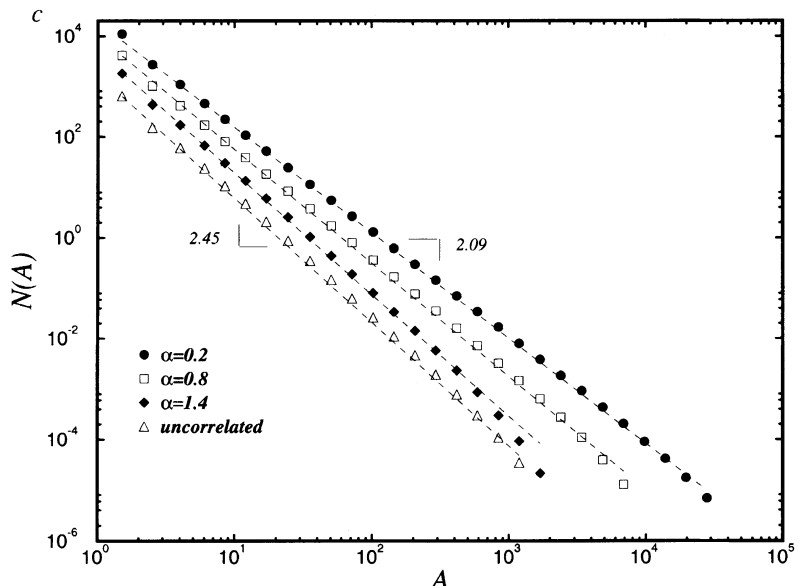
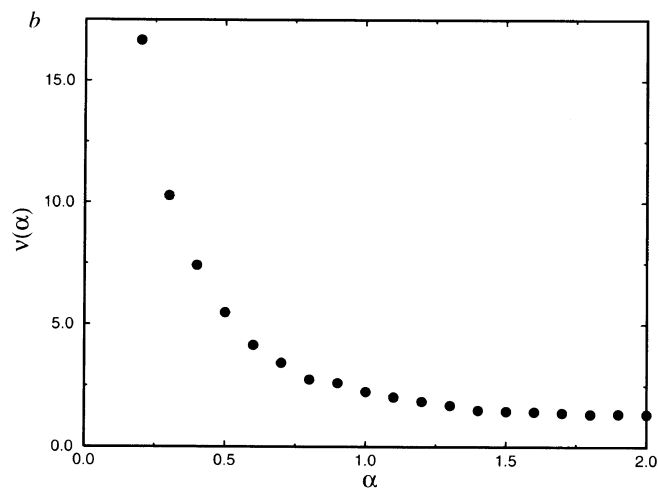
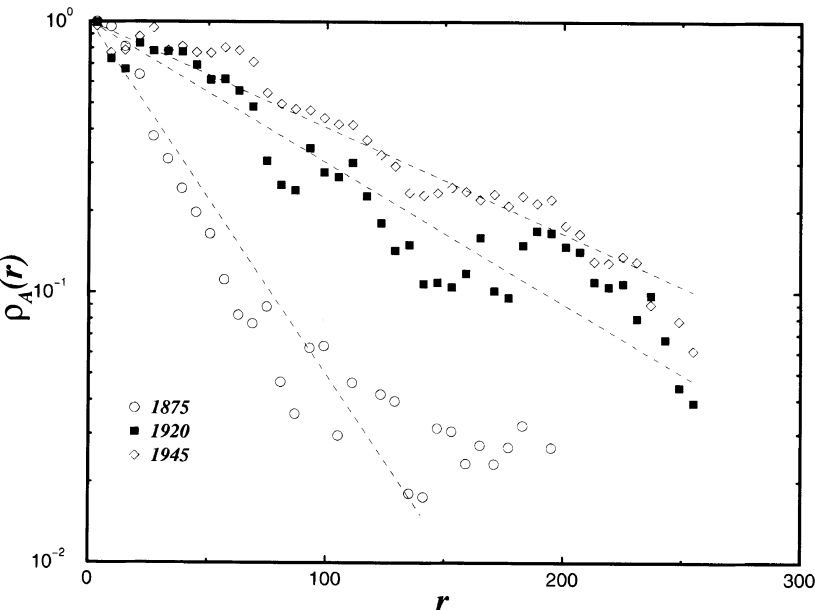


FIG. 4 Semi-log plot of the density of occupied urban areas $\rho_A(r) = e^{-\lambda r}$ for the three different stages in the growth of Berlin shown in Fig. 2a. Least-squares fits yield the results $\lambda \approx 0.030$, $\lambda \approx 0.012$, and $\lambda \approx 0.009$, respectively, showing the decrease of λ with time. We use these density profiles in the dynamical simulations of Fig. 2b. In the context of our model, this flattening pattern can be explained as follows. The model of percolation in a gradient can be related to a dynamical model of units (analogous to the development units in actual cities) diffusing from a central seed or core⁹. In this dynamical system, the units are allowed to diffuse on a two-dimensional lattice by hopping to nearest-neighbour positions. The density of units at the core remains constant: whenever a unit diffuses away from the core, it is replaced by a new unit. The density of units is analogous to $\rho_A(r)$, which in turn is proportional to⁴ the population density $\rho(r)$. A diffusion front (defined as the boundary of the cluster of units that is linked to the central core) evolves with time. The diffusion front corresponds to the urban boundary of the central city. The static properties of the diffusion front of this system were found to be the same as those predicted by the gradient percolation model⁹. Moreover, the dynamical model can explain the decrease of $\lambda(t)$ with time that is observed empirically. As the diffusion front situated around r_f moves away from the core, the city grows and the density gradient decreases because $\lambda(t) \propto 1/r_f$.

policies) is needed in order to identify the effects of planning policies on distribution of settlements. Finally, we note that only the parameter λ depends on time; possibly, future urban forms may be predicted by extrapolating λ . \square

Received 1 May; accepted 11 September 1995.

1. Batty, M. & Longley, P. *Fractal Cities* (Academic, San Diego, 1994).
2. Benguigui, L. & Daoud, M. *Geogr. Analy.* **23**, 362–368 (1991).
3. Benguigui, L. *Physica A* **219**, 13–26 (1995).
4. Witten, T. A. & Sander, L. M. *Phys. Rev. Lett.* **47**, 1400–1403 (1981).
5. Vicsek, T. *Fractal Growth Phenomena* 2nd edn (World Scientific, Singapore, 1991).



6. Coniglio, A., Nappi, C., Russo, L. & Peruggi, F. *J. Phys. A* **10**, 205–209 (1977).
 7. Makse, H. A., Havlin, S., Stanley, H. E. & Schwartz, M. *Chaos, Solitons, and Fractals* **6**, 295–303 (1995).
 8. Prakash, S., Havlin, S., Schwartz, M. & Stanley, H. E. *Phys. Rev. A* **46**, R1724–R1727 (1992).
 9. Sapoval, B., Rosso, M. & Gouyet, J.-F. *J. Phys. Lett.* **46**, 149–152 (1985).
 10. Clark, C. J. R. *Statist. Soc. A* **114**, 490–496 (1951).
 11. Gouyet, J.-F. *Physics and Fractal Structures* (Springer, Berlin, 1995).
 12. Bunde, A. & Havlin, S. (eds) *Fractals and Disordered Systems* 2nd edn (Springer, Berlin, 1996).
 13. Frankhauser, P. *La Fractalité des Structures Urbaines* (Collection Villes, Anthropos, Paris, 1994).
 14. Mills, E. S. & Tan, J. P. *Urban Studies* **17**, 313–321 (1980).
- ACKNOWLEDGEMENTS. We thank L. Benguigui, S. Buldyrev, R. Cuerno, M. Daoud, K. B. Lauritsen, S. Tomassone and S. Zapperi for their help. This work was supported by the US NSF and BP.

Quantification of pre-eruptive exsolved gas contents in silicic magmas

Paul J. Wallace*†, Alfred T. Anderson Jr* & Andrew M. Davis‡

* Department of the Geophysical Sciences, † Enrico Fermi Institute, The University of Chicago, Chicago, Illinois 60637, USA

WATER, carbon dioxide and sulphur are important in the evolution of magmas^{1,2} and the physics of volcanic eruptions^{3,4}. These volatile constituents occur in magmas as dissolved species in silicate melt, but can also form bubbles of exsolved gas if the magma is gas-saturated⁵. Quantifying the total (dissolved plus exsolved) pre-eruptive concentrations of magmatic volatiles is essential for understanding a wide range of magmatic processes. We present a method for quantifying both the amount and distribution of pre-eruptive exsolved gas in a crystallizing silicic magma body. Application to the 0.76-Myr-old⁶ Bishop rhyolitic tuff in eastern

California reveals a pre-eruptive gradient in exsolved gas, with gas contents varying from less than 2 wt% in the deeper regions of the magma body to nearly 6 wt% near the top. This gradient would have promoted stable stratification of the magma body because exsolved gas lowers bulk magma density. More generally, exsolved gas in silicic magmas could contribute to the formation of many hydrothermal ore deposits and to the fluxes of volatile species from volcanic systems.

It has commonly been assumed that silicic magmas only become gas-saturated during shallow ascent and eruption, or during the final pegmatitic stages of plutonic crystallization. But trapped inclusions of gas or fluid in volcanic phenocrysts provide direct evidence that an exsolved gas phase was present during crystallization, even in relatively crystal-poor rhyolitic magmas⁷. These inclusions provide little constraint on the mass fraction of exsolved gas in pre-eruptive magma, but remote-sensing data for volcanic SO₂ emissions suggest that many magma bodies do contain significant amounts of exsolved gas before eruption and that a large proportion of the emitted SO₂ is derived from the pre-eruptive gas phase^{8–11}.

To estimate exsolved magmatic gas contents we first focus on variations in dissolved volatiles and the physical processes by which these variations arise. Glass inclusions in phenocrysts from volcanic tephra provide a record of pre-eruptive conditions because the glass is trapped and quenched magmatic liquid that has retained its original dissolved volatile content¹². We have

† Present address: Ocean Drilling Program, Texas A&M University, College Station, Texas 77845–9547, USA.